Astronomy & Astrophysics manuscript no. LFtype˙ref2 February 2, 2008
(DOI: will be inserted by hand later)

arXiv:astro-ph/0506393v2 8 May 2006

The VIMOS VLT Deep Survey [⋆]

Evolution of the luminosity functions by galaxy type up to z=1.5 from first epoch data

E.Zucca[1], O.Ilbert[2,3], S.Bardelli[1], L.Tresse[3], G.Zamorani[1], S.Arnouts[3], L.Pozzetti[1], M.Bolzonella[2], D.Bottini[4], B.Garilli[4], V.Le Brun[3], O.Le Fèvre[3], D.Maccagni[4], J.P.Picat[5], R.Scaramella[6], M.Scodeggio[4], G.Vettolani[6], A.Zanichelli[6], C.Adami[3], M.Arnaboldi[7], A.Cappi[1], S.Charlot[8,10], P.Ciliegi[1], T.Contini[5], S.Foucaud[4], P.Franzetti[4], I.Gavignaud[5,12], L.Guzzo[9], A.Iovino[9], H.J.McCracken[10,11], B.Marano[2], C.Marinoni[9], A.Mazure[3], B.Meneux[3], R.Merighi[1], S.Paltani[3], R.Pellò[5], A.Pollo[9], M.Radovich[7], M.Bondi[6], A.Bongiorno[2], G.Busarello[7], O.Cucciati[9], L.Gregorini[6], F.Lamareille[5], G.Mathez[5], Y.Mellier[10,11], P.Merluzzi[7], V.Ripepi[7], and D.Rizzo[5]

[1] INAF-Osservatorio Astronomico di Bologna, via Ranzani 1, I-40127 Bologna (Italy)
[2] Università di Bologna, Dipartimento di Astronomia, via Ranzani 1, I-40127 Bologna (Italy)
[3] Laboratoire d'Astrophysique de Marseille (UMR 6110), CNRS-Université de Provence, BP8, F-13376 Marseille Cedex 12 (France)
[4] INAF-IASF, via Bassini 15, I-20133 Milano (Italy)
[5] Laboratoire d'Astrophysique de l'Observatoire Midi-Pyrénées (UMR 5572), 14 avenue E. Belin, F-31400 Toulouse (France)
[6] INAF-IRA, Via Gobetti 101, I-40129 Bologna (Italy)
[7] INAF-Osservatorio Astronomico di Capodimonte, via Moiariello 16, I-80131 Napoli (Italy)
[8] Max Planck Institut fur Astrophysik, D-85741 Garching bei München (Germany)
[9] INAF-Osservatorio Astronomico di Brera, via Brera 28, I-20121 Milano (Italy)
[10] Institut d'Astrophysique de Paris (UMR 7095), 98 bis Bvd Arago, F-75014 Paris (France)
[11] Observatoire de Paris, LERMA, 61 Avenue de l'Observatoire, F-75014 Paris (France)
[12] European Southern Observatory, Karl-Schwarzschild-Strasse 2, D-85748 Garching bei München (Germany)

Received – – —-; accepted – – —-

Abstract. From the first epoch observations of the VIMOS VLT Deep Survey (VVDS) up to $z = 1.5$ we have derived luminosity functions of different spectral type galaxies. The VVDS data, covering $\sim 70\%$ of the life of the Universe, allow for the first time to study from the same sample and with good statistical accuracy the evolution of the luminosity functions by galaxy type in several rest frame bands from a purely magnitude selected sample. The magnitude limit of the VVDS ($I_{AB} = 24$) is significantly fainter than the limit of other complete spectroscopic surveys and allows the determination of the faint end slope of the luminosity function with unprecedented accuracy. Galaxies have been classified in four spectral classes, from early type to irregular galaxies, using their colours and redshift, and luminosity functions have been derived in the U, B, V, R and I rest frame bands for each type, in redshift bins from $z = 0.05$ to $z = 1.5$. In all the considered rest frame bands, we find a significant steepening of the luminosity function going from early to late types. The characteristic luminosity M^* of the Schechter function is significantly fainter for late type galaxies and this difference increases in the redder bands. Within each of the galaxy spectral types we find a brightening of M^* with increasing redshift, ranging from $\lesssim 0.5$ mag for early type galaxies to ~ 1 mag for the latest type galaxies, while the slope of the luminosity function of each spectral type is consistent with being constant with redshift. The luminosity function of early type galaxies is consistent with passive evolution up to $z \sim 1.1$, while the number of bright ($M_{B_{AB}} < -20$) early type galaxies has decreased by $\sim 40\%$ from $z \sim 0.3$ to $z \sim 1.1$. We also find a strong evolution in the normalization of the luminosity function of latest type galaxies, with an increase of more than a factor 2 from $z \sim 0.3$ to $z \sim 1.3$: the density of bright ($M_{B_{AB}} < -20$) late type galaxies in the same redshift range increases of a factor ~ 6.6. These results indicate a strong type-dependent evolution and identifies the latest spectral types as responsible for most of the evolution of the UV-optical luminosity function out to $z = 1.5$.

Key words. galaxies: evolution – galaxies: luminosity function – galaxies: statistics – surveys

1. Introduction

An unbiased and detailed characterization of the luminosity function (LF) of field galaxies is a basic requirement in many extragalactic issues.

At present the local luminosity function is well constrained by the results obtained by the 2dF Galaxy Redshift Survey (2dFGRS, Norberg et al. 2002) and by the Sloan Digital Sky Survey (SDSS, Blanton et al. 2003). These surveys measure redshifts for $10^5 - 10^6$ galaxies over a large area, and therefore explore well the properties of the local ($z < 0.3$) Universe. Such large numbers of objects also allow to study the luminosity functions (as well as the correlation functions and other properties) for galaxies of different types, defined on the basis of colours and/or spectral properties. A critical analysis of the luminosity functions depending on galaxy type as measured from the various redshift surveys, as well as a comparison of the different results, can be found in de Lapparent (2003).

Madgwick et al. (2002), analyzing 2dFGRS data, find a systematic steepening of the faint end slope and a faintening of M^* of the luminosity function as one moves from passive to active star forming galaxies. Similar results are found by Blanton et al. (2001) for the SDSS sample, moving from the redder to the bluer galaxies.

For what concerns the high redshift Universe, several studies in the past ten years have aimed to map the evolution of the luminosity function. However, because of the long exposure times required to obtain spectra of high redshift galaxies, spectroscopic surveys were limited to a few 10^2 objects. The Canadian Network for Observational Cosmology field galaxy redshift survey (CNOC-2, Lin et al. 1999) and the ESO Sculptor Survey (ESS, de Lapparent et al. 2003) derived the luminosity function up to $z \sim 0.5$ using ~ 2000 and ~ 600 redshifts, respectively. de Lapparent et al. (2003) find a behaviour of the LF by type similar to the local one derived from 2dFGRS and a strong evolution of a factor 2 in the volume density of the late type galaxies with respect to the early type galaxies. Lin et al. (1999) find for early type galaxies a positive luminosity evolution with increasing redshift, which is nearly compensated by a negative density evolution. On the contrary, for late type galaxies they find a strong positive density evolution, with nearly no luminosity evolution. At higher redshift, the Canada France Redshift Survey (CFRS, Lilly et al. 1995) allowed to study the luminosity function up to $z \sim 1.1$ with a sample of ~ 600 redshifts. From this survey, the LF of the red population shows small changes with redshift, while the LF of the blue population brightens by about one magnitude from $z \sim 0.5$ to $z \sim 0.75$. Other results suggest a strong number density evolution of early type galaxies (Bell et al. 2004, Faber et al. 2006); conversely, in the K20 survey (Cimatti et al. 2002), Pozzetti et al. (2003) found that red and early type galaxies dominate the bright end of the LF and that their number density shows at most a small decrease ($< 30\%$) up to $z \sim 1$ (see also Saracco et al. 2006 and Caputi et al. 2006).

Luminosity function estimates at higher redshift and/or with larger samples are up to now based only on photometric redshifts, like the COMBO-17 survey (Wolf et al. 2003) and the analysis of the FORS Deep Field (FDF, Gabasch et al. 2004) and the Hubble Deep Fields (HDF-N and HDF-S, see e.g. Sawicki et al. 1997; Poli et al. 2001, 2003); most of these projects derived also the luminosity function for different galaxy types. Wolf et al. (2003) find that early type galaxies show a decrease of a factor ~ 10 in ϕ^* up to $z = 1.2$. Latest type galaxies show a brightening of about one magnitude in M^* and a ϕ^* increase of a factor ~ 1.6 in their highest redshift bin ($z \sim 1.1$) in the blue band. Giallongo et al. (2005), using HDFs data, find that the B band number densities of red and blue galaxies have a different evolution, with a strong decrease of the red population at $z = 2-3$ and a corresponding increase of the blue population. Dahlen et al. (2005), using GOODS data, claim that the starburst population fraction increases with redshift by a factor of 3 at $z = 2$ in the U band.

Although photometric redshifts represent a powerful tool for deep surveys, their precision strongly relies on the number of used photometric bands, on the templates and on the adopted training procedure; moreover, they are af-

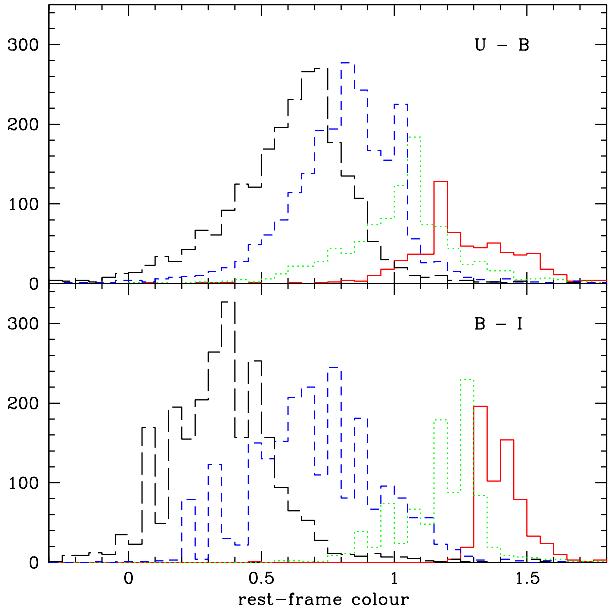

Fig. 1. Rest frame $U - B$ (upper panel) and $B - I$ (lower panel) colours for galaxies of different types: type 1 (solid line), type 2 (dotted line), type 3 (short dashed line), type 4 (long dashed line).

Send offprint requests to: Elena Zucca e-mail: `elena.zucca@oabo.inaf.it`

[*] based on data obtained with the European Southern Observatory Very Large Telescope, Paranal, Chile, program 070.A-9007(A), and on data obtained at the Canada-France-Hawaii Telescope, operated by the CNRS of France, CNRC in Canada and the University of Hawaii

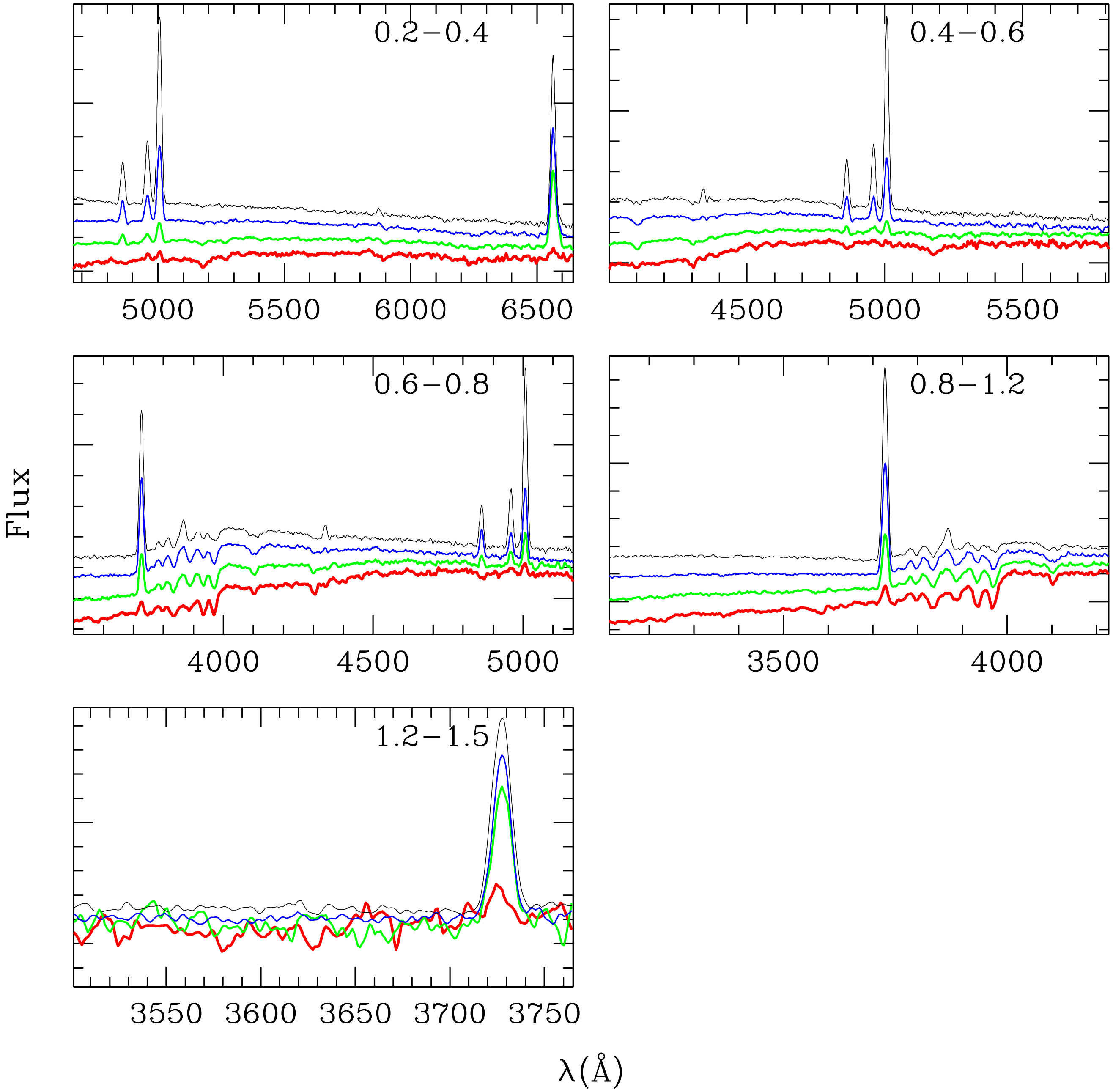

Fig. 2. Co-added VVDS spectra of galaxies of the four different types in various redshift bins, shown in rest frame wavelength. The different types are indicated with different line strengths: the ligther the line, the later the galaxy type. The redshift bin is indicated in the label of each panel. The flux on the y-axis is in arbitrary units and the spectra of the various types are arbitrarily rescaled for clarity.

fected by the problem of "catastrophic errors", i.e. objects with a large difference between the spectroscopic and the photometric redshift.

A major improvement in this field is obtained with the VIMOS VLT Deep Survey (VVDS, Le Fèvre et al. 2003b) and the DEEP-2 Galaxy Redshift Survey (Davis et al. 2003). The VVDS is an ongoing program to map the evolution of galaxies, large scale structures and AGNs from the redshift measurements of $\sim 10^5$ objects down to a magnitude $I_{AB} = 24$, in combination with a multiwavelength dataset from radio to X-rays.

From the analysis of the evolution of the global luminosity function from the first epoch VVDS data (Ilbert et al. 2005), we found a significant brightening of the M^* parameter in the U, B, V, R and I rest frame bands, going from $z = 0.05$ to $z = 2$. Moreover, we measured an increase of the comoving density of bright galaxies: this increase depends on the rest frame band, being higher in

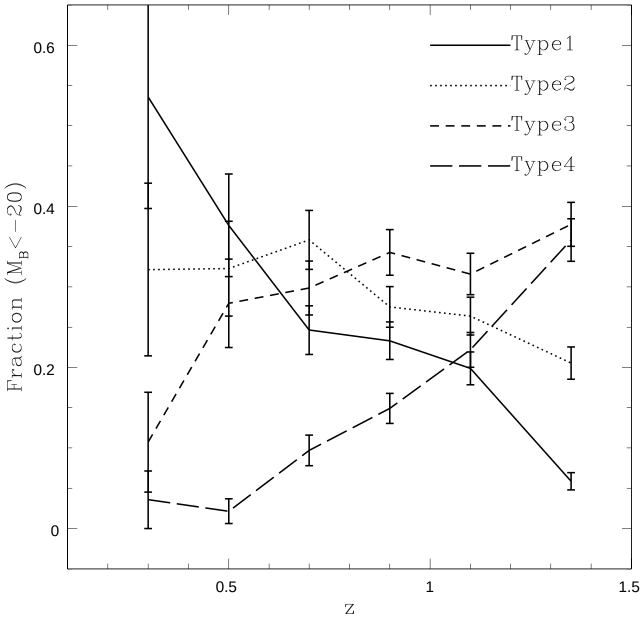

Fig. 3. Observed fraction of bright galaxies ($M_{B_{AB}} - 5log(h) < -20$) of different types as a function of redshift. Error bars are 1σ Poisson errors.

the bluest bands.

Among the other results of this survey, we recall the study of the radio selected objects (Bondi et al. 2003) and of their optical counterparts (Ciliegi et al. 2005), the evolution of the clustering properties (Le Fèvre et al. 2005b, Pollo et al. 2005) and of the bias parameter (Marinoni et al. 2005). Moreover, from the joined GALEX-VVDS sample, we derived the evolution of the far UV luminosity function (Arnouts et al. 2005) and luminosity density (Schiminovich et al. 2005).

In this paper we study the evolution of the luminosity functions of galaxies of different spectral types based on the VVDS data. This sample allows to perform this analysis for the first time with excellent statistical accuracy over a large redshift range ($0.05 < z < 1.5$).

The plan of the paper is the following: in sect. 2 we briefly present the first epoch VVDS sample, in sect. 3 we describe the galaxy classification and in sect. 4 we illustrate the method we used to estimate the luminosity functions. In sect. 5 we compare the luminosity functions of the different galaxy types and in sect. 6 we show the evolution with redshift of the luminosity functions by type. Finally in sect. 7 we compare our results with previous literature estimates and in sect. 8 we summarize our results.

Throughout the paper we adopt the cosmology $\Omega_m = 0.3$ and $\Omega_\Lambda = 0.7$, with $h = H_0/100$ km s^{-1} Mpc^{-1}, Magnitudes are given in the AB system and are expressed in the five standard bands U (Bessel), B and V (Johnson), R and I (Cousins).

2. The first epoch VVDS sample

The VVDS is described in detail in Le Fèvre et al. (2005a): here we report only the main characteristics of the sample used for the analysis presented in this paper.

The entire VVDS is formed by a wide part on 4 fields (which is not used in this paper), and by a deep part, with spectroscopy in the range $17.5 \leq I_{AB} \leq 24$ on the field 0226-04. Multicolour photometry is available for each field (Le Fèvre et al. 2004a): in particular, the B, V, R, I photometry for the 0226-04 deep field is described in detail in McCracken et al. (2003). Moreover, U band (Radovich et al. 2004) and J and K band (Iovino et al. 2005) data are available for smaller areas of these fields.

Starting from these photometric catalogues, spectroscopic observations were performed with the VIsible Multi–Object Spectrograph (VIMOS, Le Fèvre et al. 2003a) mounted on the ESO Very Large Telescope (UT3). The selection of objects for spectroscopic observations was based only on magnitude, without any other colour or shape criteria.

Deep spectroscopic observations ($17.5 \leq I_{AB} \leq 24$) were performed also on the Chandra Deep Field South (VVDS-CDFS, Le Fèvre et al. 2004b), starting from the EIS I band photometry and astrometry (Arnouts et al. 2001). Multicolour U, B, V, R and I photometry for this sample is available from the COMBO-17 survey (Wolf et al. 2003).

Spectroscopic data were reduced with the VIMOS Interactive Pipeline Graphical Interface (VIPGI, Scodeggio et al. 2005, Zanichelli et al. 2005) and redshift measurements were performed with the KBRED package (Scaramella et al. 2006) and then visually checked. Each redshift measurement was assigned a quality flag, ranging from 0 (failed measurement) to 4 (100% confidence level); flag 9 indicates spectra with a single emission line, for which multiple solutions are possible. Further details on the quality flags are given in Le Fèvre et al. (2005a).

The analysis presented in this paper is based on the first epoch VVDS deep sample, which has been obtained from the first observations (fall 2002) on the fields VVDS-02h and VVDS-CDFS, which cover 1750 and 450 arcmin^2, respectively. We eliminated from the sample spectroscopically confirmed stars and broad line AGNs, remaining with 6477 + 1236 galaxy spectra with secure spectroscopic identification (flag 2, 3, 4, 9), corresponding to a confidence level higher than 75%. Redshifts with flags 0 and 1 are taken into account statistically (see sect. 4). This spectroscopic sample, which is purely magnitude selected, has a median redshift of ~ 0.76.

3. Galaxy classification

Galaxies have been classified using all the multicolour information available; in the VVDS-02h field B, V, R and I band magnitudes are available for all galaxies, while U band data are available for 83% of the galaxies. For the

VVDS-CDFS sample U, B, V, R and I photometry from the COMBO-17 survey is used.

Absolute magnitudes are computed following the method described in the Appendix of Ilbert et al. (2005). The K-correction is computed using a set of templates and all the photometric information (UBVRI) available. However, in order to reduce the template dependency, the rest frame absolute magnitude in each band is derived using the apparent magnitude from the closest observed band, redshifted at the redshift of the galaxy. With this method, the applied K-correction is as small as possible as possible.

For each galaxy the rest frame magnitudes were matched with the empirical set of SEDs described in Arnouts et al. (1999), composed of four observed spectra (CWW, Coleman et al. 1980) and two starburst SEDs computed with GISSEL (Bruzual & Charlot 1993). The match is performed minimizing a χ^2 variable on these templates at the spectroscopic redshift of each galaxy. The same procedure has been applied by Lin et al. (1999) to the CNOC-2 survey up to $z \sim 0.55$. This approach is also similar to that adopted by Wolf et al. (2003) for the COMBO-17 survey, but we have the advantage of using spectroscopic redshifts, while they had to rely on photometric redshifts.

Galaxies have been divided in four types, corresponding to the E/S0 template (type 1), early spiral template (type 2), late spiral template (type 3) and irregular template (type 4). These types are based on the four CWW templates: type 4 includes also the two starburst templates. The numbers of galaxies for each type are listed in Table 1.

In order to have an idea of the correspondence of these types with colours, we report here the rest frame colours for each template: type 1, 2, 3 and 4 have $B_{AB} - I_{AB}$ =1.58, 1.11, 0.79 and 0.57, respectively. Given these colours, a rough colour subdivision for each class is $1.3 < B_{AB} - I_{AB}$ for type 1, $0.95 < B_{AB} - I_{AB} < 1.3$ for type 2, $0.68 < B_{AB} - I_{AB} < 0.95$ for type 3 and $B_{AB} - I_{AB} < 0.68$ for type 4. However, we remind that these colour ranges are only indicative and our classification scheme is based on the whole multicolour coverage. In Fig.1 we show the $U - B$ and $B - I$ colour distributions for the galaxies of our sample divided according to type. From this figure it is clear that, although the different types have different colour distributions, they present significant overlaps. This fact is a consequence of classification schemes using template fitting on multicolour data.

Note that, in order to avoid to be model dependent, we did not apply to the templates any correction aimed at taking into account colour evolution with redshift. It is well known that the colour of a simple stellar population subject to passive evolution was bluer in the past. In principle, this could imply that galaxies classified as type 1 at low redshift might be classified differently at higher redshift. Indeed, this effect has been invoked by the authors who found negative evolution in the luminosity function of "red" galaxies (see f.i. Wolf et al. 2003). In order to verify this hypothesis, we applied our classification scheme to synthetic spectra (Bruzual & Charlot 1993) of ellipticals (i.e. simple stellar populations and exponentially declining star formation with time scales of 0.1 Gyr and 0.3 Gyr) with formation redshift between z_{form} =2 and 20. We find that all ellipticals with $z_{form} > 2$ would be classified as type 1 objects, even at $z \sim 1$.

Table 1. Numbers of galaxies of different types in the sample

Type	N$_{gal}$
total	7713
type 1	730
type 2	1290
type 3	2622
type 4	3071

In order to check, at least on a statistical basis, the consistency between this photometric classification and average spectral properties, we summed the normalized spectra of all galaxies in each of the four types. The resulting average spectra are shown in Fig.2 for each type in various redshift bins. This figure confirms the robustness of our classification scheme: moving from type 1 to type 4 objects, the composite spectra show an increasingly blue continuum, with emission lines of increasing strength. This confirms that the four types show different spectral features and therefore represent different classes of objects.

For the VVDS-CDFS sample, HST-ACS images are available. Using these data, Lauger et al. (2006) classified the galaxies in this sample using an asymmetry-concentration diagram. Plotting our type 1 galaxies in this diagram, we find that $\sim$ 91% of them lie in the region of bulge dominated objects, showing an excellent consistency also between our photometric classification and a morphological one.

In Fig.3 we plot the observed fraction of bright galaxies of each type as a function of redshift. We selected objects with $M_{B_{AB}} - 5log(h) < -20$ because these galaxies are visible in the whole redshift range. From this figure it is clear the growing importance of bright late type objects with increasing redshift and the corresponding strong decrease of the fraction of bright early type galaxies.

4. Luminosity function estimate

Luminosity functions were derived using the Algorithm for Luminosity Function (ALF), a dedicated tool which uses various estimators: the non-parametric $1/V_{max}$ (Schmidt 1968), C^+ (Lynden Bell 1971), $SWML$ (Efstathiou et al. 1988) and the parametric STY (Sandage, Tammann & Yahil 1979), for which we assumed a Schechter function (Schechter 1976). The tool and these estimators, as well as their specific use in the context of the VVDS, are described in detail in Ilbert et al. (2005).

Ilbert et al. (2004) have shown that the estimate of the global luminosity function can be biased, mainly in its

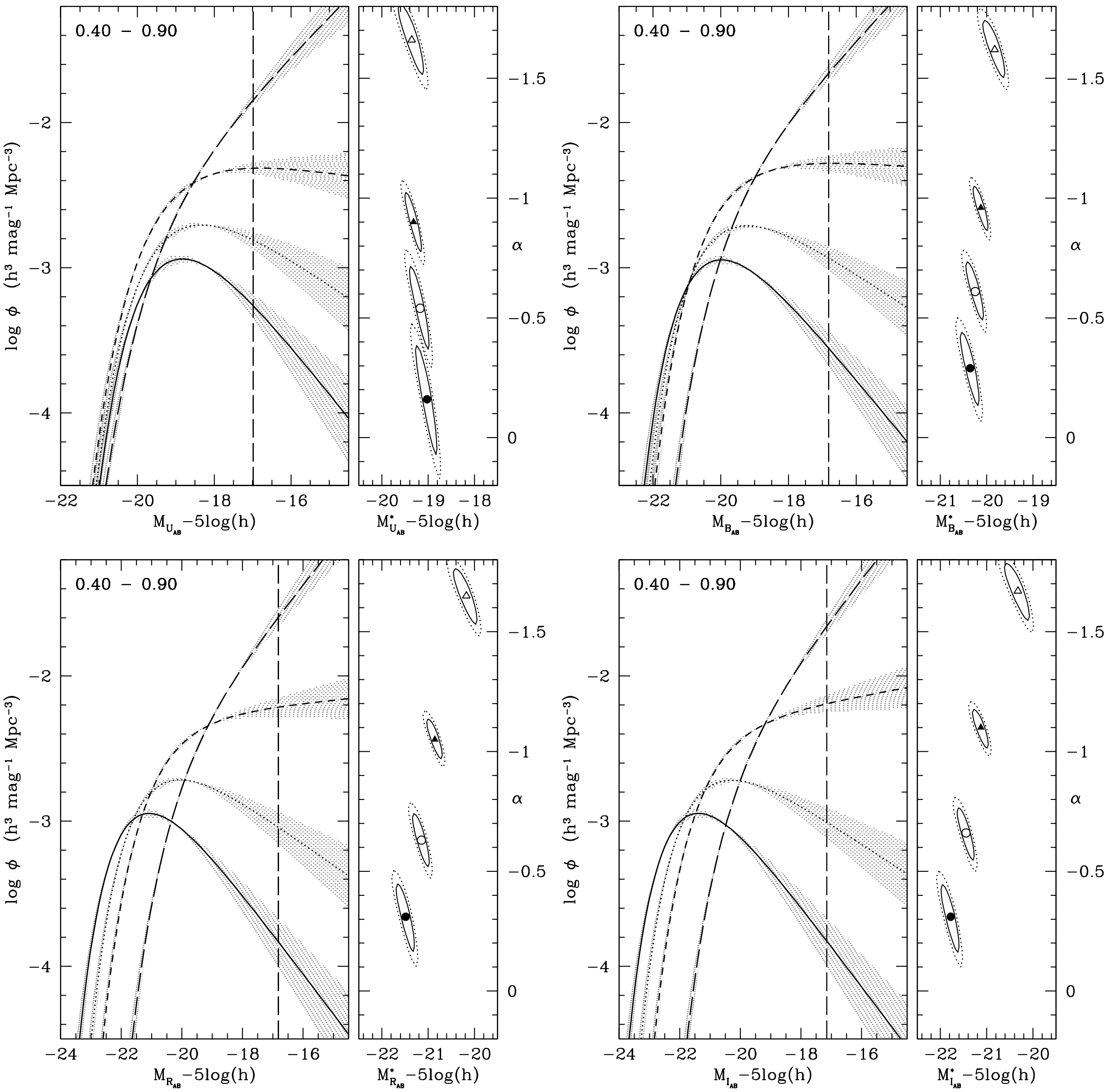

Fig. 4. Luminosity functions by different types in the redshift range $[0.4-0.9]$ in various rest frame bands: upper panels U (left) and B (right); lower panels R (left) and I (right). Note that the ranges of magnitude are different in the various panels. The lines represent the *STY* estimates for type 1 (solid), type 2 (dotted), type 3 (short dashed) and type 4 (long dashed) galaxies. The vertical dashed line represents the faint absolute magnitude limit considered in the *STY* estimate (see text). The shaded regions represent the 68% uncertainties on the parameters α and M^*, whose confidence ellipses are reported in the right panels. The ellipse contours are at 68% and 90% confidence level (solid and dotted line respectively). The points inside the ellipses represent the best fit values for type 1 (filled circle), type 2 (open circle), type 3 (filled triangle) and type 4 (open triangle) galaxies.

faint end, when the band in which it is measured is far from the rest frame band in which galaxies are selected. This is due to the fact that, because of the K-corrections, different galaxy types are visible in different absolute magnitude ranges at a given redshift. When computing the global luminosity functions (Ilbert et al. 2005), we avoided this bias by using for the *STY* estimate, in each redshift range, only galaxies within the absolute magnitude range where all the SEDs are potentially observable.
Even if this bias is much less important when estimating the luminosity function of galaxies divided by types, we have, however, taken it into account. The absolute magnitude limits for the *STY* estimate are indicated with vertical dashed lines in the figures, and in the tables where the best fit parameters are reported (Table 2 and 3) we give both the total number of objects and the number of galaxies within this magnitude limit.

In order to take into account the unknown redshifts (not

Table 2. *STY* parameters (with 1σ errors) for different galaxy types in different bands in the redshift range $[0.4-0.9]$

				Ω_m=0.3	Ω_Λ=0.7	
Band	Type	Number$^{(a)}$	Number$^{(b)}$	α	$M^*_{AB}-5log(h)$	$\phi^*(10^{-3}h^3Mpc^{-3})$
U	1	411	357	$-0.16^{+0.15}_{-0.15}$	$-19.03^{+0.14}_{-0.15}$	$3.35^{+0.20}_{-0.26}$
	2	677	596	$-0.54^{+0.12}_{-0.11}$	$-19.18^{+0.13}_{-0.14}$	$4.83^{+0.48}_{-0.53}$
	3	1371	1192	$-0.90^{+0.08}_{-0.08}$	$-19.31^{+0.11}_{-0.12}$	$7.32^{+0.86}_{-0.86}$
	4	1442	1238	$-1.66^{+0.10}_{-0.10}$	$-19.35^{+0.17}_{-0.18}$	$4.09^{+1.21}_{-1.04}$
B	1	411	404	$-0.29^{+0.10}_{-0.10}$	$-20.35^{+0.13}_{-0.13}$	$3.19^{+0.23}_{-0.26}$
	2	677	669	$-0.61^{+0.08}_{-0.08}$	$-20.25^{+0.12}_{-0.12}$	$4.48^{+0.43}_{-0.44}$
	3	1371	1349	$-0.96^{+0.06}_{-0.06}$	$-20.12^{+0.10}_{-0.11}$	$6.79^{+0.72}_{-0.71}$
	4	1442	1403	$-1.62^{+0.08}_{-0.08}$	$-19.83^{+0.15}_{-0.16}$	$4.46^{+1.08}_{-0.95}$
V	1	411	411	$-0.31^{+0.09}_{-0.09}$	$-21.13^{+0.12}_{-0.13}$	$3.16^{+0.23}_{-0.25}$
	2	677	677	$-0.61^{+0.07}_{-0.07}$	$-20.82^{+0.11}_{-0.12}$	$4.51^{+0.40}_{-0.41}$
	3	1371	1371	$-1.00^{+0.06}_{-0.06}$	$-20.57^{+0.10}_{-0.11}$	$6.21^{+0.66}_{-0.64}$
	4	1442	1442	$-1.62^{+0.08}_{-0.08}$	$-20.03^{+0.15}_{-0.16}$	$4.36^{+1.03}_{-0.92}$
R	1	411	411	$-0.31^{+0.09}_{-0.09}$	$-21.48^{+0.12}_{-0.13}$	$3.16^{+0.23}_{-0.25}$
	2	677	677	$-0.63^{+0.07}_{-0.07}$	$-21.15^{+0.11}_{-0.12}$	$4.37^{+0.40}_{-0.41}$
	3	1371	1371	$-1.05^{+0.05}_{-0.05}$	$-20.86^{+0.11}_{-0.11}$	$5.55^{+0.63}_{-0.60}$
	4	1442	1436	$-1.65^{+0.08}_{-0.08}$	$-20.18^{+0.16}_{-0.17}$	$3.87^{+0.99}_{-0.87}$
I	1	411	411	$-0.31^{+0.09}_{-0.09}$	$-21.78^{+0.12}_{-0.13}$	$3.17^{+0.23}_{-0.25}$
	2	677	677	$-0.66^{+0.07}_{-0.07}$	$-21.44^{+0.12}_{-0.12}$	$4.22^{+0.40}_{-0.40}$
	3	1371	1370	$-1.10^{+0.05}_{-0.05}$	$-21.13^{+0.11}_{-0.11}$	$5.05^{+0.60}_{-0.57}$
	4	1442	1413	$-1.67^{+0.08}_{-0.08}$	$-20.32^{+0.17}_{-0.18}$	$3.58^{+0.97}_{-0.86}$

(a) Number of galaxies in the redshift bin

(b) Number of galaxies brighter than the bias limit (sample used for *STY* estimate; see the text for details)

observed objects and failed spectra), a weight was applied to each galaxy, following the procedure described in detail in Ilbert et al. (2005).

This weight is a combination of two different contributions: the target sampling rate and the spectroscopic success rate. The target sampling rate, i.e. the fraction of observed galaxies, corrects for the selection effects due to the procedure used for the mask preparation (Bottini et al. 2005): to maximize the number of slits, the procedure tends to select objects with smaller angular size on the x-axis of the image, corresponding to the direction in which the slits are placed. As a consequence, the final spectroscopic sample has a bias against large objects, which produces a mild dependence of the target sampling rate on the apparent magnitude. The target sampling rate is $\sim 25\%$ for most of the sample and is computed as a function of the object size (see Ilbert et al. 2005 for further details). The spectroscopic success rate takes into account the fraction of objects without a good redshift determination (i.e. flags 0 and 1). As shown in Ilbert et al. (2005), these objects are expected to have a different redshift distribution with respect to that of the sample with measured redshift, as confirmed by the use of their photometric redshifts. Given the fact that the spectroscopic success rate decreases for faint apparent magnitudes, we derived it in four magnitude bins as a function of redshift (using photometric redshifts, see Fig.3 in Ilbert et al. 2005). The shape of the spectroscopic success rate is similar in all magnitude bins, showing a maximum at $z \sim 0.7$ and two minima for $z < 0.5$ and $z > 1.5$. Since the number of galaxies for each type is not large enough to reliably estimate the spectroscopic success rate as a function also of the galaxy type, we have used the global spectroscopic success rate for all galaxy types.

In order to check the effect of the "cosmic variance", i.e. variations in the luminosity function due to fluctuations in the large scale structure, we applied the following test on the VVDS-02h deep area. For this field we derived photometric redshifts (Ilbert et al. 2006) based on both VVDS photometry (BVRIJK) and on new CFHT Legacy Survey photometry (ugriz), which has now become available in a field covering 1 sq. deg. (http://www.cfht.hawaii.edu/Science/CFHLS/) which includes the 1700 arcmin^2 area covered by the VVDS spectroscopic survey. Then we divided the field in two non overlapping regions (the sub-area where spectroscopic data are available and the remaining area) and we compared the luminosity distributions of galaxies in these two samples (~0.5 sq.deg. each), in the same redshift bins in which the luminosity functions were derived. In each redshift bin the two distributions show average differences of the order of 10%, with some larger fluctuations due to Poisson statistics, without any systematic trend. Therefore the influence of the "cosmic variance" is expected to be limited.

5. Comparison of the luminosity functions of different types

As a first step, we compare the luminosity functions for galaxies of different types, in order to see which is the relative behaviour of the various populations. To perform this comparison, we selected galaxies in the redshift range $[0.4-0.9]$. About 50% of the objects of our sample are included in this redshift interval, covering a wide range of luminosities (i.e. absolute magnitudes in the B band are in the range $[-23.7; -16.8] - 5\log(h)$). Moreover, the spectroscopic success rate of our survey reaches a maximum at $z \sim 0.7$ and therefore the possible dependency of the estimated LF on the weighting scheme described above is minimized in this redshift interval.

In Fig.4 we report the luminosity functions estimated with the STY method in the rest frame bands U, B, R and I, with the corresponding confidence ellipses for the α and M^* parameters. The values of the parameters with their 1σ errors, as well as the number of galaxies for each type, are reported in Table 2. The ϕ^* parameters listed in this table are derived adopting the density estimator of Efstathiou et al. (1988), following the procedure described in the Appendix of Ilbert et al. (2005).

Table 2 shows that our estimates are based on several hundreds of galaxies for each type, and are therefore well statistically constrained, as can be seen also from the sizes of the confidence ellipses in the figures. The first, very clear result which appears from Fig.4 is the significant strong steepening of the luminosity functions going from early to late types. In all bands the power law slope steepens by $\Delta\alpha \sim 1.3-1.5$ going from type 1 to type 4 galaxies and galaxies of late types are the dominant population at faint magnitudes.

Systematic trends are also seen in the M^* parameter. In the reddest bands (lower panels in Fig.4), M^* is significantly fainter for late type galaxies and this faintening is particularly apparent for type 4 objects. The brighter M^* for early type galaxies reflects the fact that most of the more massive objects belong to this population.

The difference of the M^* values for different types decreases in the B band and disappears or even changes sign in the U band. This behaviour is explained by the fact that the luminosity in the bluer bands is dominated by the light of young stars, produced during the star formation activity. Galaxies of later types, which are still actively forming stars, are therefore more luminous in the bluer bands.

These results are qualitatively in agreement with previous results from the literature, most of which at lower redshift (see de Lapparent 2003 for a review of the results from a number of surveys in the redshift range $0 \le z \le 0.6$). In particular, in almost all surveys the luminosity function of late type galaxies is steeper and with a fainter M^* with respect to that of early type galaxies. However, a quantitative comparison with previous results is difficult, because of the different classification schemes adopted in the various surveys, the different redshift ranges and selection criteria.

6. Evolution with redshift of the luminosity functions by type

We derived luminosity functions for each type in redshift bins in the U, B, V, R and I rest frame bands. Given our multicolour coverage and the explored redshift range, the estimate of the absolute magnitudes in the U and B rest frame bands are those which require less extrapolations (see Appendix A and Figure A.1 in Ilbert et al. 2005). Therefore, to limit the number of figures in the paper, we show the results in the B rest frame band.

Figures 5, 6, 7 and 8 show the luminosity function for type 1, 2, 3 and 4 galaxies in redshift bins, obtained with C^+ and STY methods. The luminosity functions derived with the other two methods ($1/V_{max}$ and $SWML$) are consistent with those shown in the figures, but are not drawn for clarity. The dotted line in each panel represents the fit derived in the redshift range $[0.4-0.9]$ (see previous section), while the dashed line is the estimate derived by fixing the slope α to the value obtained in the range $[0.4-0.9]$.

In Table 3 we report the Schechter parameters, with their 1σ errors, estimated for the various redshift bins, from $z = 0.2$ to $z = 1.5$ for each type; as a reference, in the last line we give the parameters derived in the redshift bin $[0.4-0.9]$.

We do not show the results for bins where the number of objects is too small (less than ~ 30) to constrain the parameters of the luminosity function (these are the bin $[0.05-0.2]$ for type 1 and 2 and the bin $[1.2-1.5]$ for type 1). Given the bright magnitude limit of the survey ($I_{AB} \ge 17.5$) and the small sampled volume, bright galaxies are not sampled in the redshift bin $[0.05-0.2]$ and therefore we can not constrain the M^* parameter even for type 3 and 4 galaxies, where the number of objects is relatively high (~ 80). For this reason we show in the figures the luminosity function estimates in this bin, but we do not report the STY parameters for this redshift range in Table 3.

In Fig.9 we show the confidence ellipses of the parameters α and M^* in different redshift bins for the different types. From this figure it is possible to see that, within each type, the estimated slopes α in the various redshift bins are always consistent (within 90% confidence level) with each other and with the value derived in the redshift range $[0.4-0.9]$. Therefore, there is no evidence of a significant change with redshift of the luminosity function slope within each galaxy type. Note also that the uncertainties on the slope estimates become quite large for $z > 1$: this is due to the fact that, even with the faint limit ($I_{AB} \le 24$) of this survey, the number of galaxies fainter than M^* is too low to well constrain the slope.

In each panel of Figures 5, 6, 7 and 8 we draw, as a reference, the luminosity function derived in the redshift bin $[0.4-0.9]$ (dotted line). Comparing this curve with the estimates of the luminosity function in the different redshift bins an evolution can be seen, strongly depending on the galaxy type. This evolution is particularly evident for type 4 galaxies: going from low to high redshift there

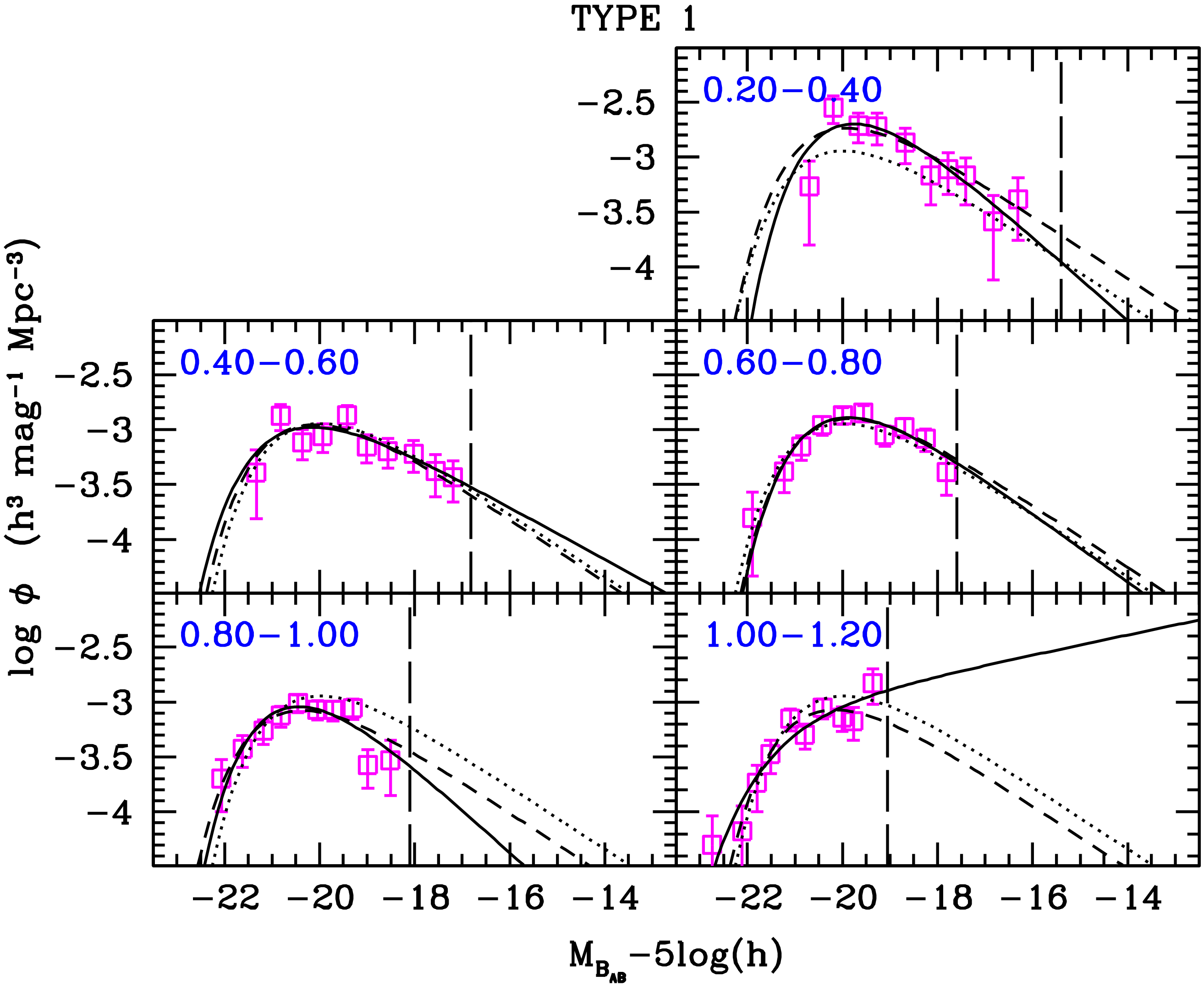

Fig. 5. Evolution of the luminosity function in the B-band for type 1 galaxies. Each panel refers to a different redshift bin, which is indicated in the label. The vertical dashed line represents the faint absolute limit considered in the *STY* estimate. The luminosity functions are estimated with different methods (see text for details) but for clarity we plot only the results from C^+ (open squares), and *STY* (solid line). The dashed line is the *STY* estimate obtained by fixing α to the value determined in the redshift range $[0.4-0.9]$. The dotted line represents the luminosity function estimated in the redshift range $[0.4-0.9]$: this curve is reported in each panel as a reference.

is an almost continuous brightening of M^* and at fixed luminosity the density of these galaxies was much higher in the past.

The observed evolution of the luminosity function could be due to an evolution in luminosity and/or in density or both. One of the advantages of the *STY* method is that of allowing to derive the α and M^* parameters independently from ϕ^*, which is not possible when one directly fits a Schechter function on the $1/V_{max}$ points.

Given the fact that we found that α is consistent with being constant for each type, we can fix it at the reference value derived in the redshift range $[0.4-0.9]$ and then study the variations of the parameters M^* and ϕ^* as a function of the redshift (see upper and middle panels of Fig.10). These estimates are reported in Table 3.

From Fig.10 we can see a mild evolution of M^* from the lowest to the highest redshift bin for each type. In particular, this brightening ranges from $\lesssim 0.5$ mag for early type galaxies to ~ 1 mag for the latest type galaxies. The only exception with respect to the general trend is that of type 3 objects in the bin $[0.2-0.4]$, for which the best fit value of the M^* parameter is significantly fainter than expexted. The reason for this discontinuity in M^* for type 3 galaxies at low redshift is not clear.

On the contrary, the ϕ^* parameter shows a very different behaviour for type 1, 2 and 3 galaxies with respect to type 4 galaxies. The first three types show a rapid decrease of ϕ^* at low redshifts (between $z \sim 0.3$ and $z \sim 0.5$), then ϕ^* remains roughly constant up to $z \sim 0.9$ and finally slowly decreases up to $z = 1.5$.

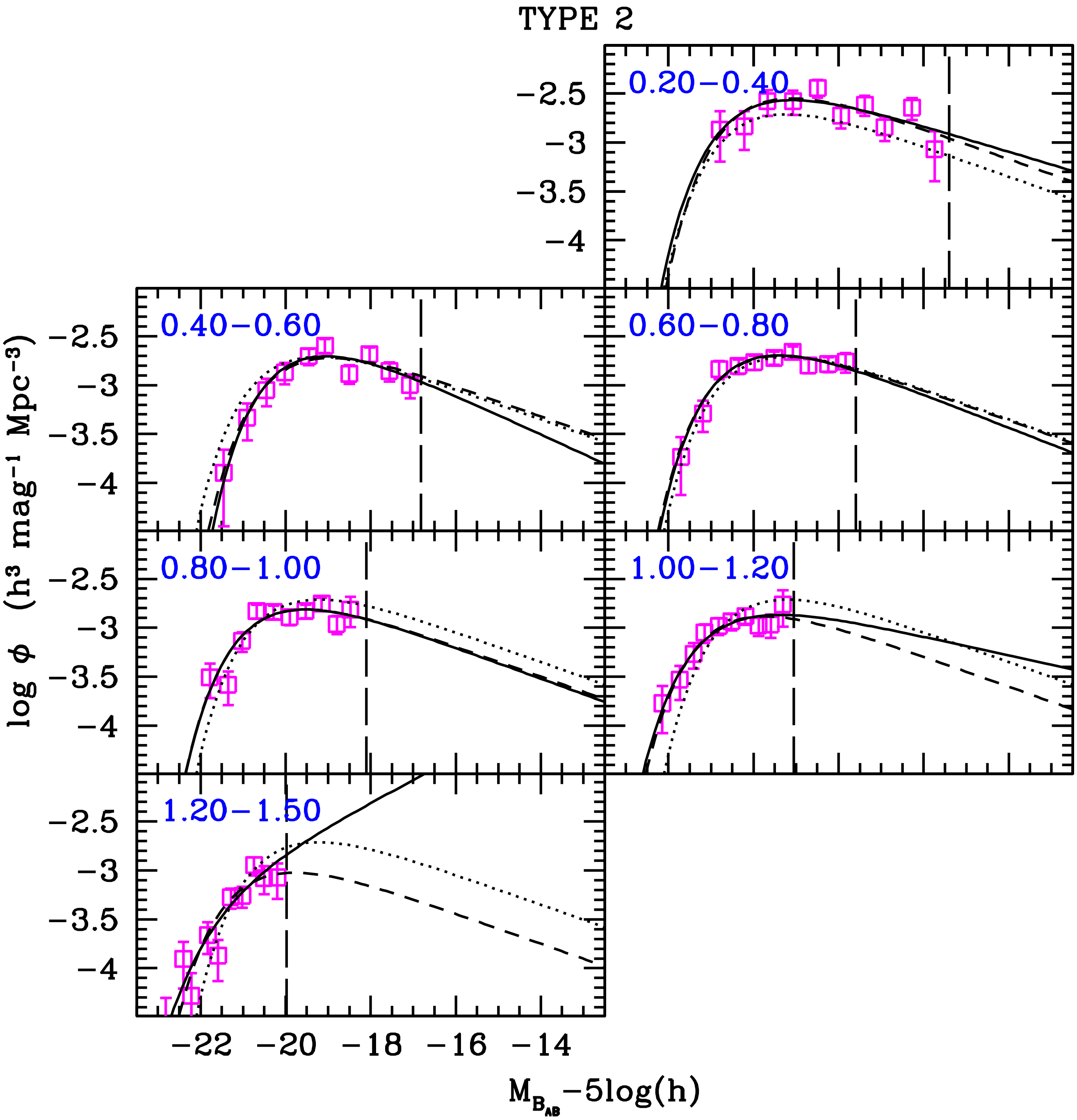

Fig. 6. Evolution of the luminosity function in the B-band for type 2 galaxies. The meaning of the lines and the symbols is the same as in Fig.5.

Type 4 objects, on the contrary, show an increase in ϕ^* at low redshift, then ϕ^* is nearly constant up to $z \sim 0.8$ and shows a rapid increase of a factor ~ 2 at $z = 1.1$. Then there seems to be a decrease from $z = 1.1$ to $z = 1.3$. However, this decrease can likely be a spurious effect, due to the fact that in this bin the estimated M^* is very close to the bias limit (see Sect. 4). If, for example, we fix M^* to the value obtained in the previous redshift bin $[1.0 - 1.2]$, we derive a significantly higher value for ϕ^*, i.e. $\phi^* = 5.83 \times 10^{-3} h^3 Mpc^{-3}$ (corresponding to $\phi^*/\phi^*_{ref} = 1.31$). Therefore the last ϕ^* value for type 4 galaxies is likely to be a lower limit of the true density value.

This analysis of the different trends with redshift of the ϕ^* parameter indicates that the importance of type 4 galaxies is increasing with redshift. However, since M^* is changing with redshift (see above), the trends of ϕ^* can not be immediately interpreted in terms of density at a given absolute magnitude. For this reason, we have computed the density of bright galaxies as a function of redshift. We integrated the best fit luminosity function down to $M_{B_{AB}} - 5log(h) < -20$. This limit approximately corre-

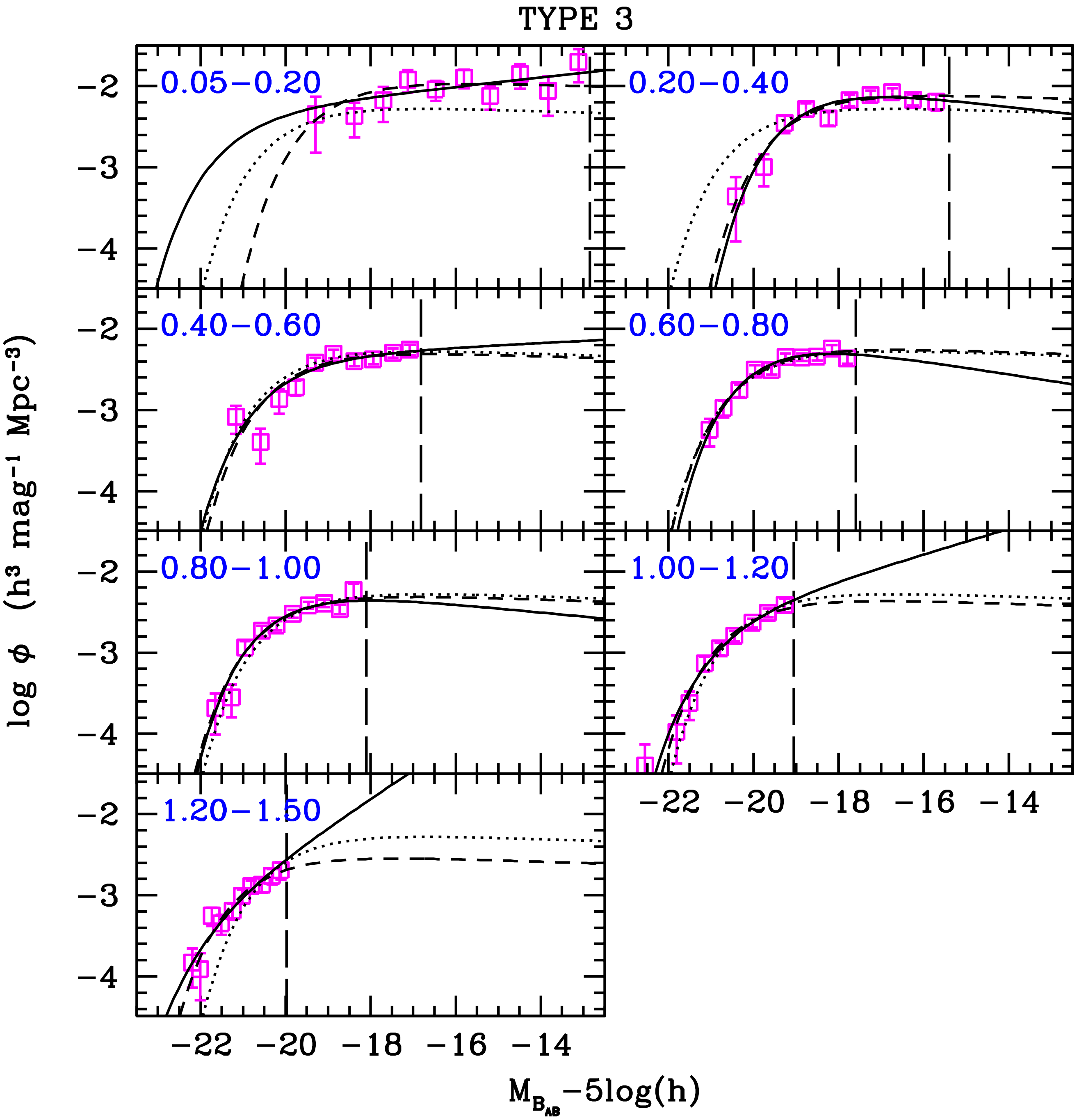

Fig. 7. Evolution of the luminosity function in the B-band for type 3 galaxies. The meaning of the lines and the symbols is the same as in Fig.5.

sponds to the faintest galaxies which are visible in the whole redshift range. In the lowest panel of Fig.10 we plot the density of bright galaxies of each type as a function of redshift.

The main results shown in this plot can be summarized in the following way:

a. the density of bright early type galaxies (type 1) decreases with increasing redshift, however this decrease is rather modest, being of the order of ∼ 40% from $z \sim 0.3$ to $z \sim 1.1$;

b. the density of bright late type galaxies (type 4) is instead significantly increasing, by a factor ∼ 6.6 from $z \sim 0.3$ to $z \sim 1.3$.

The behaviour of type 4 galaxies is also responsible of the evolution of the global luminosity function measured by Ilbert et al. (2005). In fact, the increasing number of both faint and bright type 4 galaxies leads to the steepening of the global LF (due to the very steep slope of type 4 LF) and to the brightening of M^* (due to the increasing fraction of bright blue objects). This fact has been directly checked summing the LF of all types and comparing the result with the global LF estimate.

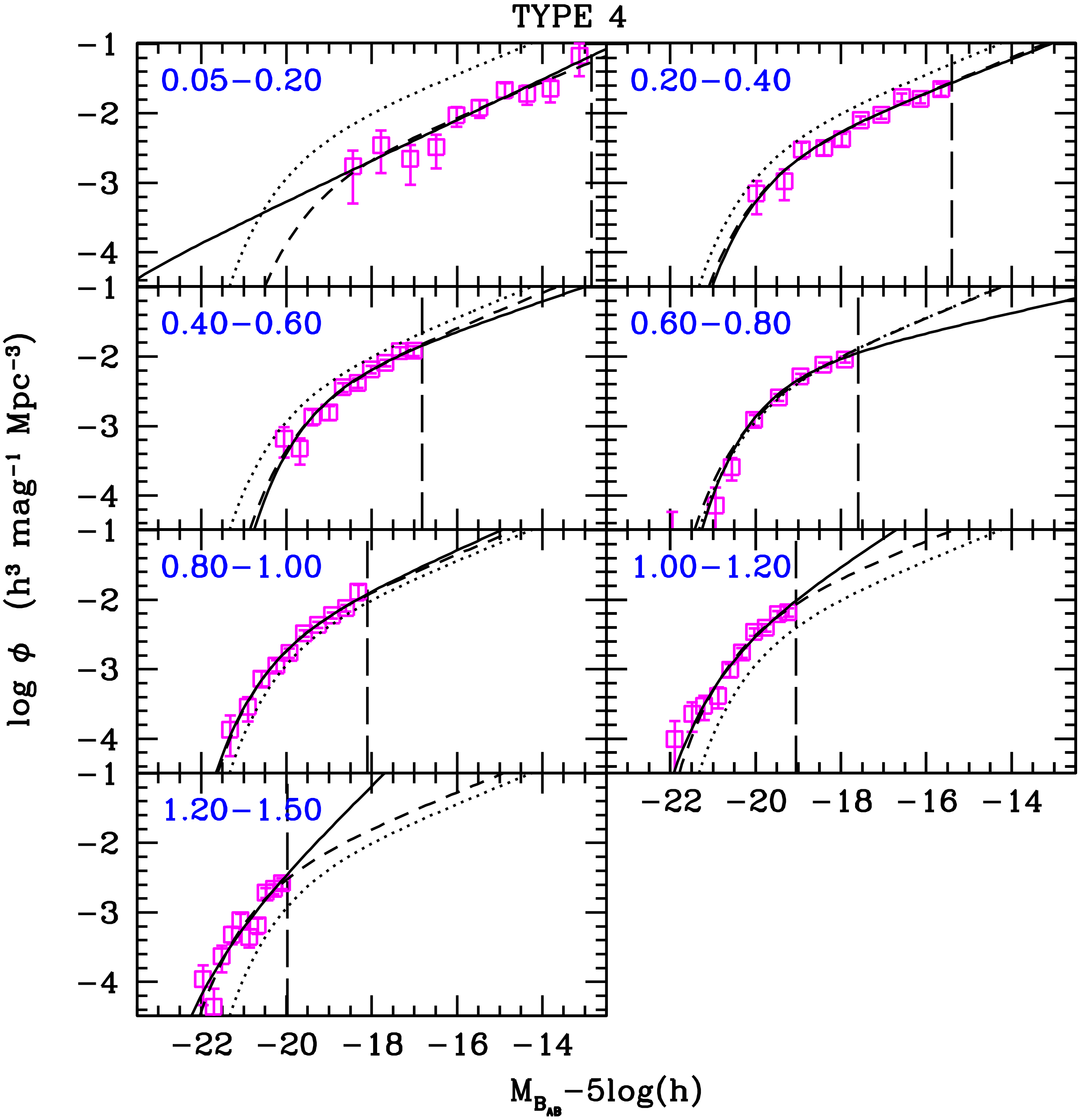

Fig. 8. Evolution of the luminosity function in the B-band for type 4 galaxies. The meaning of the lines and the symbols is the same as in Fig.5.

7. Comparison with previous literature results

Although various estimates of the luminosity function by galaxy type are available in the literature, a quantitative comparison of our results with previous analyses is not straightforward, because of the different classification schemes adopted in the various surveys, the different numbers of galaxy types, the different redshift ranges and selection criteria.

The strong density evolution of late type galaxies we find in the redshift range $[0.2 - 1.5]$ extends to significantly higher redshift the results found by de Lapparent et al. (2004) for their latest type at $z \sim 0.5$.

Among the other surveys, CNOC-2 (Lin et al. 1999) and COMBO-17 (Wolf et al. 2003) adopted a classification scheme somewhat similar to ours. Lin et al. (1999) divided their sample of galaxies with $z < 0.55$ in three classes (early, intermediate and late type) using CWW templates. For early type galaxies they found a positive luminosity evolution, which is nearly compensated by a negative density evolution. On the contrary, for late type galaxies they found a strong positive density evolution,

Table 3. *STY* parameters (with 1σ errors) for different galaxy types in the rest frame B band

				Ω_m=0.3	Ω_Λ=0.7			
Type	z-bin	Number$^{(a)}$	Number$^{(b)}$	α	$M^*_{AB} - 5log(h)$		ϕ^* $(10^{-3}h^3Mpc^{-3})$	
					α free /	α fixed	α free /	α fixed
1	0.20-0.40	70	65	$-0.04^{+0.28}_{-0.27}$	$-19.81^{+0.39}_{-0.46}$	$-20.27^{+0.27}_{-0.31}$	$5.90^{+0.73}_{-0.73}$	$5.15^{+0.64}_{-0.64}$
	0.40-0.60	113	106	$-0.40^{+0.20}_{-0.20}$	$-20.71^{+0.39}_{-0.46}$	$-20.49^{+0.17}_{-0.18}$	$2.81^{+0.50}_{-0.58}$	$3.12^{+0.30}_{-0.30}$
	0.60-0.80	204	197	$-0.22^{+0.17}_{-0.17}$	$-20.14^{+0.19}_{-0.20}$	$-20.22^{+0.09}_{-0.10}$	$3.70^{+0.33}_{-0.43}$	$3.53^{+0.25}_{-0.25}$
	0.80-1.00	164	164	$-0.01^{+0.25}_{-0.24}$	$-20.46^{+0.22}_{-0.24}$	$-20.73^{+0.11}_{-0.12}$	$2.68^{+0.21}_{-0.21}$	$2.36^{+0.18}_{-0.18}$
	1.00-1.20	114	114	$-1.23^{+0.34}_{-0.34}$	$-21.49^{+0.48}_{-0.57}$	$-20.53^{+0.11}_{-0.12}$	$0.92^{+0.65}_{-0.56}$	$2.39^{+0.22}_{-0.22}$
	0.40-0.90	411	404	$-0.29^{+0.10}_{-0.10}$	$-20.35^{+0.13}_{-0.13}$		$3.19^{+0.23}_{-0.26}$	
2	0.20-0.40	136	132	$-0.67^{+0.13}_{-0.13}$	$-20.29^{+0.37}_{-0.44}$	$-20.13^{+0.19}_{-0.21}$	$5.88^{+1.34}_{-1.33}$	$6.50^{+0.56}_{-0.56}$
	0.40-0.60	203	195	$-0.50^{+0.15}_{-0.14}$	$-19.81^{+0.20}_{-0.21}$	$-19.97^{+0.12}_{-0.12}$	$4.99^{+0.74}_{-0.79}$	$4.35^{+0.31}_{-0.31}$
	0.60-0.80	322	310	$-0.57^{+0.13}_{-0.13}$	$-20.33^{+0.19}_{-0.20}$	$-20.39^{+0.09}_{-0.10}$	$4.81^{+0.69}_{-0.74}$	$4.58^{+0.26}_{-0.26}$
	0.80-1.00	267	267	$-0.60^{+0.20}_{-0.20}$	$-20.54^{+0.24}_{-0.26}$	$-20.55^{+0.10}_{-0.11}$	$3.58^{+0.64}_{-0.74}$	$3.54^{+0.22}_{-0.22}$
	1.00-1.20	178	175	$-0.76^{+0.34}_{-0.33}$	$-20.92^{+0.35}_{-0.40}$	$-20.77^{+0.12}_{-0.13}$	$2.64^{+0.79}_{-0.98}$	$3.01^{+0.23}_{-0.23}$
	1.20-1.50	103	103	$-1.57^{+0.61}_{-0.62}$	$-21.65^{+0.62}_{-0.84}$	$-20.82^{+0.13}_{-0.14}$	$0.81^{+1.04}_{-0.72}$	$2.19^{+0.22}_{-0.22}$
	0.40-0.90	677	669	$-0.61^{+0.08}_{-0.08}$	$-20.25^{+0.12}_{-0.12}$		$4.48^{+0.43}_{-0.44}$	
3	0.20-0.40	341	329	$-0.84^{+0.10}_{-0.10}$	$-18.92^{+0.19}_{-0.21}$	$-19.14^{+0.12}_{-0.13}$	$12.37^{+2.30}_{-2.20}$	$9.82^{+0.54}_{-0.54}$
	0.40-0.60	451	429	$-1.07^{+0.10}_{-0.10}$	$-20.28^{+0.24}_{-0.27}$	$-20.04^{+0.11}_{-0.11}$	$4.93^{+1.26}_{-1.17}$	$6.31^{+0.30}_{-0.30}$
	0.60-0.80	626	610	$-0.79^{+0.13}_{-0.13}$	$-19.86^{+0.17}_{-0.19}$	$-20.10^{+0.09}_{-0.09}$	$9.10^{+1.46}_{-1.51}$	$7.11^{+0.29}_{-0.29}$
	0.80-1.00	534	533	$-0.87^{+0.15}_{-0.15}$	$-20.23^{+0.18}_{-0.19}$	$-20.33^{+0.08}_{-0.08}$	$7.01^{+1.29}_{-1.34}$	$6.27^{+0.27}_{-0.27}$
	1.00-1.20	292	288	$-1.39^{+0.26}_{-0.26}$	$-20.82^{+0.31}_{-0.34}$	$-20.38^{+0.10}_{-0.10}$	$3.11^{+1.56}_{-1.35}$	$5.57^{+0.33}_{-0.33}$
	1.20-1.50	208	193	$-1.86^{+0.55}_{-0.59}$	$-21.87^{+0.77}_{-1.23}$	$-20.81^{+0.12}_{-0.13}$	$0.80^{+1.82}_{-0.79}$	$3.67^{+0.27}_{-0.27}$
	0.40-0.90	1371	1349	$-0.96^{+0.06}_{-0.06}$	$-20.12^{+0.10}_{-0.11}$		$6.79^{+0.72}_{-0.71}$	
4	0.20-0.40	394	380	$-1.59^{+0.11}_{-0.12}$	$-19.60^{+0.46}_{-0.58}$	$-19.73^{+0.29}_{-0.33}$	$3.05^{+2.09}_{-1.67}$	$2.59^{+0.13}_{-0.13}$
	0.40-0.60	487	449	$-1.53^{+0.18}_{-0.19}$	$-19.17^{+0.33}_{-0.39}$	$-19.38^{+0.17}_{-0.18}$	$5.57^{+3.14}_{-2.56}$	$4.10^{+0.19}_{-0.19}$
	0.60-0.80	656	622	$-1.35^{+0.15}_{-0.15}$	$-19.55^{+0.20}_{-0.21}$	$-19.95^{+0.12}_{-0.12}$	$7.72^{+2.33}_{-2.09}$	$4.07^{+0.16}_{-0.16}$
	0.80-1.00	552	552	$-1.68^{+0.20}_{-0.21}$	$-20.19^{+0.31}_{-0.36}$	$-20.10^{+0.12}_{-0.12}$	$4.06^{+2.44}_{-1.93}$	$4.72^{+0.20}_{-0.20}$
	1.00-1.20	389	373	$-1.99^{+0.33}_{-0.34}$	$-20.62^{+0.41}_{-0.52}$	$-20.19^{+0.12}_{-0.12}$	$3.19^{+3.49}_{-2.22}$	$6.95^{+0.36}_{-0.36}$
	1.20-1.50	239	188	$-2.50^{+0.52}_{-0.91}$	$-21.58^{+0.76}_{-0.40}$	$-20.53^{+0.12}_{-0.12}$	$0.52^{+2.06}_{-0.29}$	$4.34^{+0.32}_{-0.32}$
	0.40-0.90	1442	1403	$-1.62^{+0.08}_{-0.08}$	$-19.83^{+0.15}_{-0.16}$		$4.46^{+1.08}_{-0.95}$	

(a) Number of galaxies in the redshift bin
(b) Number of galaxies brighter than the bias limit (sample used for *STY* estimate; see the text for details)

with nearly no luminosity evolution. We see at higher redshift the same trend in density, but our evolution in M^* is contained within one magnitude for each type. Wolf et al. (2003) used a sample of $\sim$ 25000 galaxies with photometric redshifts, applying a classification scheme in four classes similar to ours but using the Kinney et al. (1996) templates instead of the CWW templates.

In Figure 11 we compare our results (solid lines) with those from COMBO-17 (dashed lines). Note that, since our data extend always to fainter absolute magnitudes, in particular for type 1 galaxies, our estimates of the faint end slope are likely to be better determined: these estimates are derived in each redshift bin, while the COMBO-17 slopes are fixed to the value determined in the redshift range [0.2 - 0.4]. This figure shows that there are significant differences in both shapes and evolution of the LF estimates. The slope of the COMBO-17 LF is flatter than ours for type 1 galaxies, while it is steeper for types 2 and 3 (at least up to z = 1.0). The most significant difference between the two surveys regards the evolution of type 1 galaxies, for which we do not have any evidence of the very strong density decrease with increasing redshift present in COMBO-17 data. The reason for this difference is unclear: it could be due to the use of different templates in the definition of the galaxy types or to a degeneracy between photometric redshift and classification, which might affect the COMBO-17 data. Bell et al. (2004) explained the strong negative evolution of type 1 galaxies as a consequence of the blueing with increasing redshift of elliptical galaxies with respect to the template used for classification. In this way, at increasing redshift an increasing number of "ellipticals" would be assigned a later type, therefore producing the detected density decrease observed in COMBO-17 data. However, as already mentioned in sect.3, we verified that this effect does not affect our classification scheme, at least up to $z \sim 1$ and for simple stellar populations with $z_{form} > 2$.

As a test of this possible effect, we compared the LF obtained by adding together type 1 and 2 objects. In this way we can check whether the differences between VVDS and COMBO-17 LF of type 1 galaxies is due to the fact that a significant fraction of high redshift type 1 galaxies in COMBO-17 are classified as type 2 galaxies. This comparison is shown in Fig.12. The discrepancy between VVDS

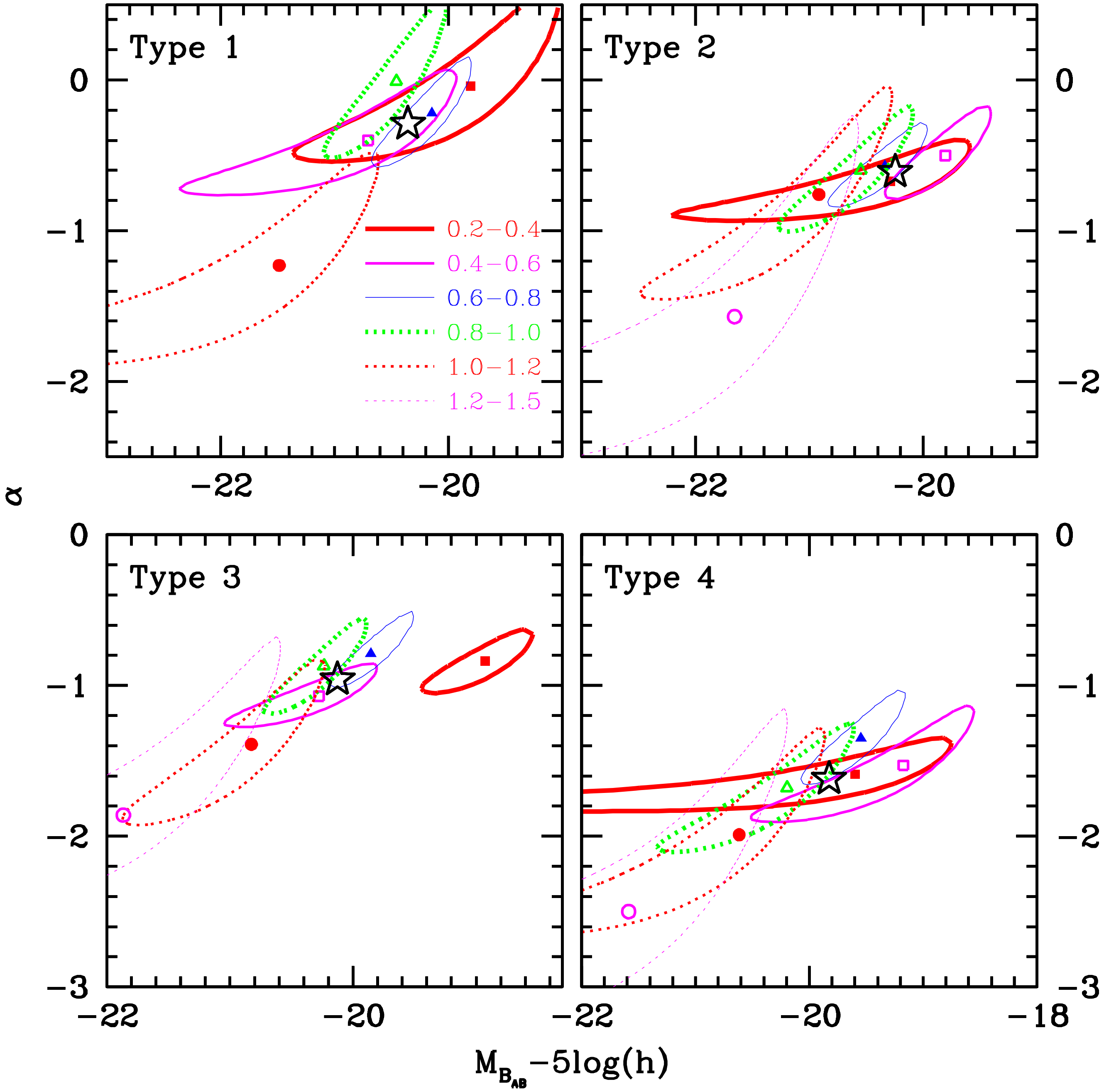

Fig. 9. Confidence ellipses at 90% confidence level for the α and M^* parameters of the luminosity functions reported in Fig.5, 6, 7 and 8. Different line types and weights refer to different redshift bins, described in the labels; the points indicate the best fit values in the redshift bins $[0.2 - 0.4]$ (filled squares), $[0.4 - 0.6]$ (open squares), $[0.6 - 0.8]$ (filled triangles), $[0.8 - 1.0]$ (open triangles), $[1.0 - 1.2]$ (filled circles), $[1.2 - 1.5]$ (open circles). The large open star indicates the reference value obtained in the redshift bin $[0.4 - 0.9]$.

and COMBO-17 LF is now reduced, but there are still significant differences both in slope (being the COMBO-17 LF steeper than that of VVDS) and in normalization, especially in the highest redshift bin, where the VVDS LF is more than a factor 2 higher than the COMBO-17 LF.

8. Conclusions

In this paper we studied the evolution of the luminosity function of different galaxy types up to $z = 1.5$, using 7713 spectra with $17.5 \le I_{AB} \le 24$ from the first epoch VVDS deep sample.

The VVDS data allow for the first time to study with excellent statistical accuracy the evolution of the luminosity

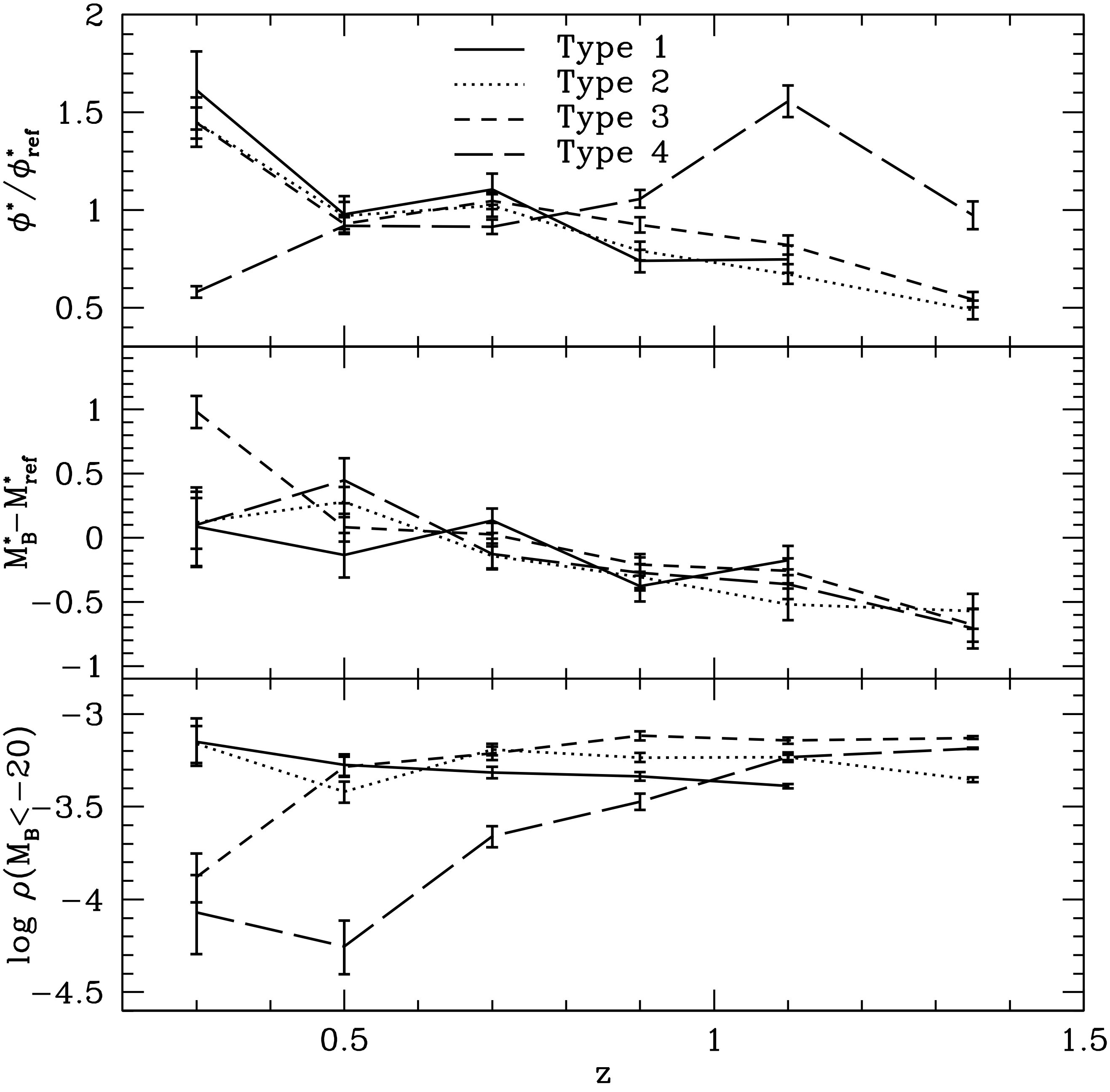

Fig. 10. Evolution of the parameters ϕ^* (upper panel) and M^* (middle panel) as a function of the redshift, for different galaxy types. In the lowest panel the density of bright ($M_{B_{AB}} - 5log(h) < -20$) galaxies of different types is shown. The slope α is fixed to the value derived in the redshift range [0.4 − 0.9]; the suffix 'ref' indicates the parameters estimated in the redshift range [0.4 − 0.9]. Error bars are at 1σ.

functions by galaxy type from relatively low redshift up to $z = 1.5$ from a single purely magnitude selected spectroscopic sample. The faint limiting magnitude of the VVDS sample allows to measure the slope of the faint end of the luminosity function with unprecedented accuracy up to $z \sim 1.2$. The use of spectroscopic redshifts implies low "catastrophic" failure rate compared to the photometric redshifts and therefore rare populations are sampled with a better accuracy, like in the bright end on the luminosity function. Moreover, the use of spectroscopic redshifts allow to classify galaxies avoiding a possible degeneracy between photometric redshift and classification.

VVDS galaxies were classified in four spectral classes using their colours and redshift, from early type to irregular galaxies, and luminosity functions were derived for each type in redshift bins, from $z = 0.05$ to $z = 1.5$, in the U, B, V, R and I rest frame bands.

We find a significant strong steepening of the luminos-

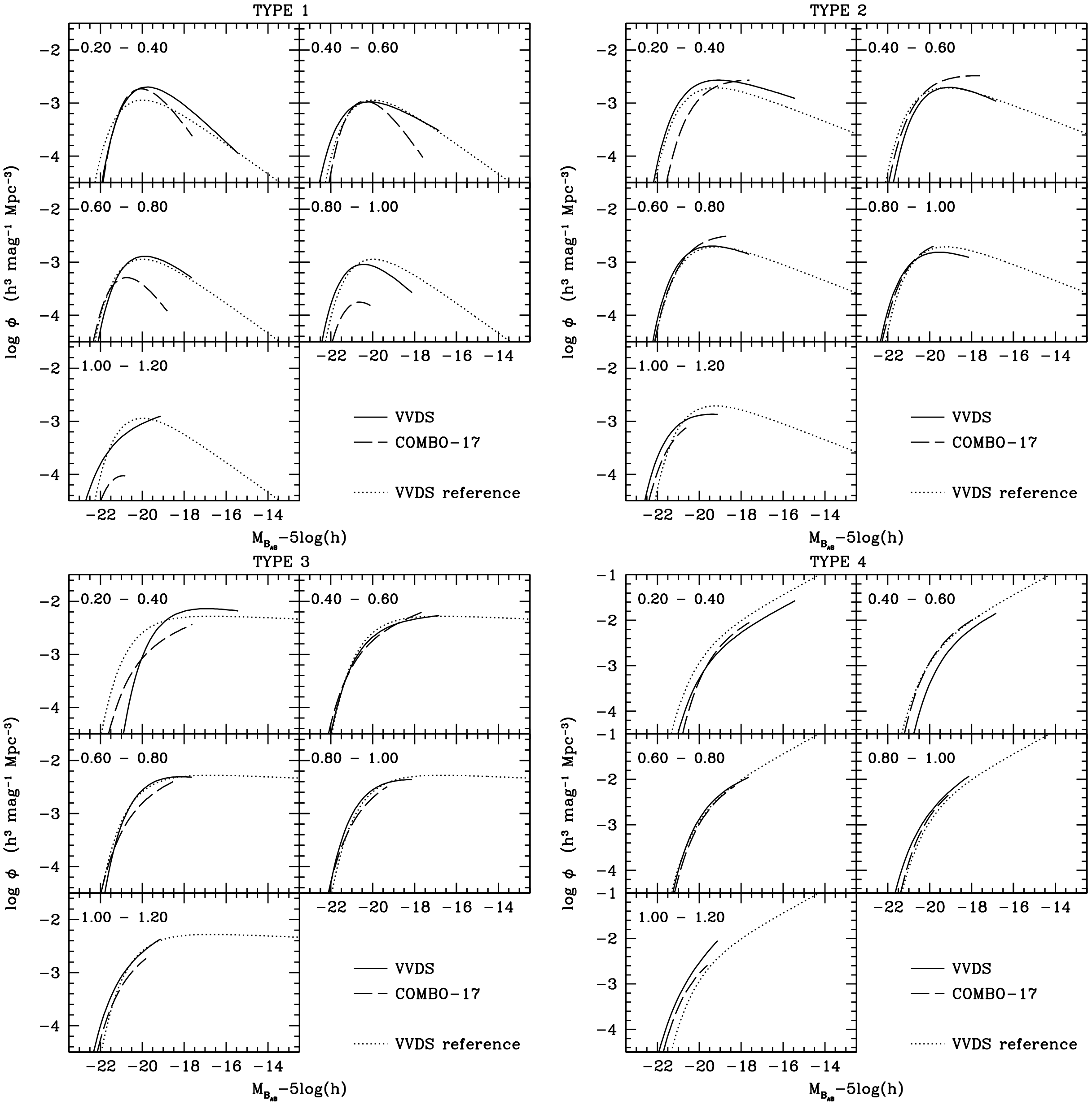

Fig. 11. Comparison between VVDS and COMBO-17 luminosity functions, in various redshift bins (indicated in the label in each panel) and for various types. Upper panels: type 1 (left) and type 2 (right) galaxies. Lower panels: type 3 (left) and type 4 (right) galaxies. Solid lines: VVDS estimate. Dotted lines: VVDS estimate in the redshift range $[0.4 - 0.9]$, plotted as a reference. Dashed line: COMBO-17 estimate from Wolf et al. (2003).

ity function going from early to late types: in all bands the power law slope steepens by $\Delta\alpha \sim 1.3 - 1.5$ going from type 1 to type 4. Moreover, the M^* parameter of the Schechter function is significantly fainter for late type galaxies. As expected, this difference increases in the redder bands, reaching ~ 1.4 mag in the I band.

Studying the variations with redshift of the luminosity function for each type, we find that there is no evidence of a significant change of the slope, while we find a brightening of M^* with increasing redshift, ranging from $\lesssim 0.5$ mag for early type galaxies to ~ 1 mag for the latest type galaxies. We also find a strong evolution in the normalization of the luminosity function of latest type galaxies, with an increase of more than a factor 2 in the ϕ^* parameter going from $z \sim 0.3$ to $z \sim 1.3$. The density of bright ($M_{B_{AB}} - 5log(h) < -20$) galaxies shows a modest decrease ($\sim 40\%$) for early type objects from $z \sim 0.3$ to $z \sim 1.1$; on the contrary, the number of bright late type galaxies increases of a factor ~ 6.6 from $z \sim 0.3$ to $z \sim 1.3$.

Our results indicate that the importance of type 4 galaxies is increasing with redshift, with an important contribution of both bright and faint blue objects. This fact is also largely responsible of the evolution of the global luminosity function measured by Ilbert et al. (2005), which shows a brightening of M^* and a steepening of α with increasing redshift. Moreover, the increasing contribution of blue

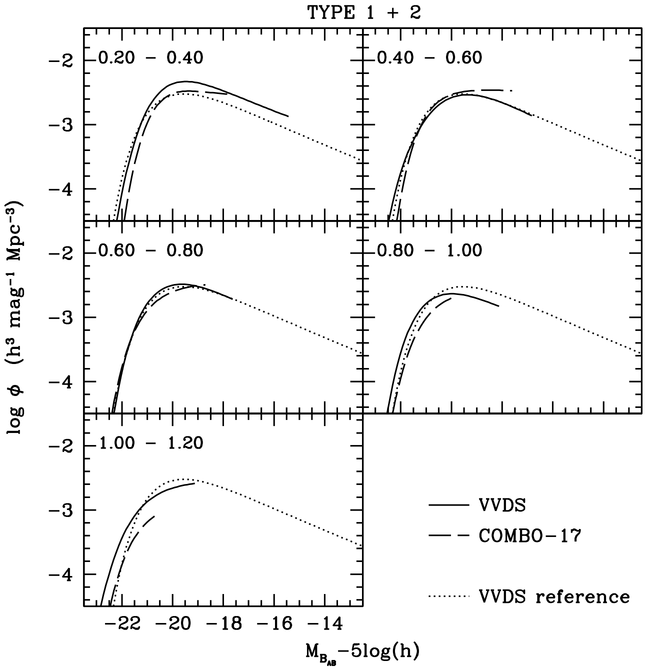

Fig. 12. Comparison between VVDS and COMBO-17 luminosity functions, in various redshift bins (indicated in the label in each panel) for the sum of types 1 and 2. The meaning of the symbols is the same as in Fig.11.

galaxies has been seen in the evolution of the GALEX-VVDS luminosity function at 1500Å(Arnouts et al. 2005). We are therefore pinpointing that the galaxies responsible for most of the evolution quoted in the literature belong to the population of the latest spectral type. The epoch at which a transition between a Universe dominated by late type galaxies and a Universe dominated by old massive objects occurs is at a redshift of $z \sim 0.7-0.8$.

The fact that type 1 galaxies show only a mild evolution both in luminosity (positive) and in density (negative) is consistent with the fact that most of the objects in this class are old ($z_{form} > 2$, see sect. 3) galaxies, experiencing only a passive evolution in the explored redshift range. More intriguing is the density evolution of type 4 galaxies, which corresponds to an increasing number of bright star forming galaxies towards high redshift which could be connected to various populations of high redshift objects seen in multiwavelength surveys.

Acknowledgements. This research has been developed within the framework of the VVDS consortium.

This work has been partially supported by the CNRS-INSU and its Programme National de Cosmologie (France), and by Italian Ministry (MIUR) grants COFIN2000 (MM02037133) and COFIN2003 (num.2003020150).

The VIMOS VLT observations have been carried out on guaranteed time (GTO) allocated by the European Southern Observatory (ESO) to the VIRMOS consortium, under a contractual agreement between the Centre National de la Recherche Scientifique of France, heading a consortium of French and Italian institutes, and ESO, to design, manufacture and test the VIMOS instrument.

References

Arnouts, S., Cristiani, S., Moscardini, L., et al. 1999, MNRAS, 310, 540

Arnouts, S., Vandame, B., Benoist, C., et al. 2001, A&A, 379, 740

Arnouts, S., Schiminovich, D., Ilbert, O., et al. 2005, ApJL, 619, L43

Bell, E.F., Wolf, C., Meisenheimer, K. et al. 2004, ApJ, 608, 752

Blanton, M.R., Dalcanton, J., Eisenstein, D., et al. 2001, AJ, 121, 2358

Blanton, M.R., Hogg, D.W., Bahcall, N.A., et al. 2003, ApJ, 592, 819

Bondi, M., Ciliegi, P., Zamorani, G., et al. 2003, A&A, 403, 857

Bottini, D., Garilli, B., Maccagni, D., et al. 2005, PASP, 117, 996

Bruzual, G., Charlot, S. 1993, ApJ, 405, 538

Caputi, K.I., McLure, R.J., Dunlop, J.S., Cirasuolo, M., Schael, A.M. 2006, MNRAS, 366, 609

Ciliegi, P., Zamorani, G., Bondi, M., et al. 2005, A&A, 441, 879

Cimatti, A., Mignoli, M., Daddi, E., et al. 2002, A&A, 392, 395

Coleman, G.D., Wu, C.C., Weedman, D.W. 1980, ApJS, 43, 393

Dahlen, T., Mobasher, B., Somerville, R., et al. 2005, ApJ, 631, 126

Davis, M., Faber, S.M., Newman, J., et al. 2003, SPIE vol.4834, p.161

de Lapparent, V., Galaz, G., Bardelli, S., Arnouts, S. 2003, A&A, 404, 831

de Lapparent, V. 2003, A&A, 408, 845

de Lapparent, V., Arnouts, S., Galaz, G., Bardelli, S. 2004, A&A, 422, 841

Efstathiou, G., Ellis, R.S., Peterson, B.A. 1988, MNRAS, 232, 431

Faber, S.M., Willmer, C.N.A., Wolf, C., et al. 2006, ApJ, submitted (astro-ph/0506044)

Gabasch, A., Bender, R., Seitz, S., et al. 2004, A&A, 421, 41

Giallongo, E., Salimbeni, S., Menci, N., et al. 2005, ApJ, 622, 116

Ilbert, O., Tresse, L., Arnouts, S., et al. 2004, MNRAS, 351, 541

Ilbert, O., Tresse, L., Zucca, E., et al. 2005, A&A, 439, 863

Ilbert, O., et al. 2006, A&A, submitted (astro-ph/0603217)

Iovino, A., McCracken, H.J., Garilli, B., et al. 2005, A&A, 442, 423

Kinney, A.L., Calzetti, D., Bohlin, R.C., et al. 1996, ApJ, 467, 38

Lauger, S., Ilbert, O., Burgarella, D., et al. 2006, A&A, in press

Le Fèvre, O., Vettolani, G., Maccagni, D., et al. 2003a, SPIE, vol. 4841, p.1670

Le Fèvre, O., et al. 2003b, proc. of IAU Symp. 216, Maps of the Cosmos, Sydney, July 2003, M.Colless & L.Staveley-Smith eds., in press (astro-ph/0311475)

Le Fèvre, O., Mellier, Y., McCracken, H.J., et al. 2004a, A&A, 417, 839

Le Fèvre, O., Vettolani, G., Paltani, S., et al. 2004b, A&A, 428, 1043

Le Fèvre, O., Vettolani, G., Garilli, B., et al. 2005a, A&A, 439, 845

Le Fèvre, O., Guzzo, L., Meneux, B., et al. 2005b, A&A, 439, 877
Lilly, S.J., Tresse, L., Hammer, F., Crampton, D., Le Fèvre, O. 1995, ApJ, 455, 108
Lin, H., Yee, H.K.C., Carlberg, R.G., et al. 1999, ApJ, 518, 533
Lynden Bell, D. 1971, MNRAS, 155, 95
Madgwick, D., Lahav, O., Baldry, I.K., et al. 2002, MNRAS, 333, 133
Marinoni, C., Le Fèvre, O., Meneux, B., et al. 2005, A&A, 442, 801
McCracken, H.J., Radovich, M., Bertin, E., et al. 2003, A&A, 410, 17
Norberg, P., Cole, S., Baugh, C.M., et al. 2002, MNRAS, 336, 907
Poli, F., Menci, N., Giallongo, E., et al. 2001, ApJL, 551, L45
Poli, F., Giallongo, E., Fontana, A., et al. 2003, ApJL, 593, L1
Pollo, A., Meneux, B., Guzzo, L., et al. 2005, A&A, 439, 887
Pozzetti, L., Cimatti, A., Zamorani, G., et al. 2003, A&A, 402, 837
Radovich, M., Arnaboldi, M., Ripepi, V., et al. 2004, A&A, 417, 51
Sandage, A., Tammann, G.A., Yahil, A. 1979, ApJ, 232, 352
Saracco, P., Fiano, A., Chincarini, G., et al. 2006, MNRAS, in press (astro-ph/0512147)
Sawicki, M.J., Lin, H., Yee, H.K.C. 1997, AJ, 113, 1
Scaramella, R. et al. 2006, in preparation
Schechter, P. 1976, ApJ, 203, 297
Schiminovich, D., Ilbert, O., Arnouts, S., et al. 2005, ApJL, 619, L47
Schmidt, M. 1968, ApJ, 151, 393
Scodeggio, M., Franzetti, P., Garilli, B., et al. 2005, PASP, 117, 1284
Tresse, L., et al. 2006, A&A, submitted
Wolf, C., Meisenheimer, K., Rix, H.W., et al. 2003, A&A, 401, 73
Zanichelli, A., Garilli, B., Scodeggio, M., et al. 2005, PASP, 117, 1271